Journal of Applied Polymer Science

Creep and Recovery Behavior of Kenaf/Polypropylene Nonwoven Composites

Ayou Hao,[1] Yizhuo Chen,[2] Jonathan Y. Chen[1,3]
[1]Materials Science and Engineering Program, The University of Texas at Austin, Austin, Texas 78712
[2]College of Textiles, North Carolina State University, Raleigh, North Carolina 27695
[3]School of Human Ecology, The University of Texas at Austin, Austin, Texas 78712
Correspondence to: A. Hao (E-mail: ayouhao@utexas.edu)

ABSTRACT: This article reports an exploratory study on the creep and recovery behavior of kenaf/polypropylene nonwoven composites (KPNCs), serving as a bio-based substitution for polypropylene (PP) plastics in the automotive industry due to the environmental concern. The creep and recovery behavior of KPNC and solid virgin PP were performed by dynamic mechanical analyzer (DMA) which allowed it to be studied extensively. The linear viscoelastic limit (LVL) was found at 1 MPa. Two popular creep models, the four-element Burgers (FEB) model and the Findley power law (FPL) model, were used to model the creep behavior in this study. The FEB model was found only appropriate for characterizing short-term creep behavior. In contrast, the FPL model was satisfactory for predicting the long-term creep performance. The long-term creep behavior of KPNC in comparison to virgin PP plastic was predicted using the time-temperature superposition (TTS) principle. The 1-year creep strains were estimated to be 0.32% for KPNC and 1.00% for virgin PP at 40°C. A three-day creep test was conducted to validate the effectiveness of the TTS prediction. KPNC showed a better creep resistance and higher recoverability than the virgin PP, especially in a high-temperature environment. © 2014 Wiley Periodicals, Inc. J. Appl. Polym. Sci. **2014**, *131*, 40726.

KEYWORDS: cellulose and other wood products; composites; mechanical properties; properties and characterization; thermal properties

Received 5 January 2014; accepted 15 March 2014
DOI: 10.1002/app.40726

INTRODUCTION

Natural Fiber Nonwoven Composites

Kenaf/polypropylene nonwoven composites (KPNCs) are ideal for producing bio-based automotive interior parts because they can reduce vehicle weight for higher fuel efficiency; lower production cost by time and energy saving; enhance vehicle acoustical performance; and improve passenger safety.[1] Consequently, KPNC is nowadays increasingly used as a substitute for petroleum-based injection-molded plastics and glass fiber–reinforced composites in auto interior manufacture, such as passenger carpet, door panel trim, headliner, trunk trim, and so on.[1] Expanded use of these green materials will bring environmental benefits in terms of carbon sequestration,[2] greenhouse gas reduction,[3] and an increase of vehicle fuel efficiency.[4]

Nonwoven fabrication followed by compression molding has some advantages over resin transfer molding[5] and injection molding.[6] It is a one-shot process with reduced processing time for thermoplastic polymers, energy saving, and cost effectiveness.[7,8] However, little attention has been paid to the nonwoven fabrication and compression molding technique for producing KPNCs used in this research. There is also little work on characterization of the nonwoven composite mechanical and thermal behavior that is distinct from traditional metal or plastic materials. This article reports an exploratory study on the creep performance of KPNCs comparing to solid virgin polypropylene (PP) plastics. Because PP is a standard plastic currently used in the automotive interior application,[9] this study intends to explore the application of KPNC as a bio-based substitution for PP plastics used in the automotive industry. The strain rate effects that studied in our previous article[10] confirmed the time-dependence of KPNCs. The creep and recovery behavior of nonwoven structured natural fiber composites is very distinct from solid virgin PP, because KPNC has a high volume fraction of pores. KPNC also has a different microstructure from solid PP. Compared to solid virgin, PP has only one phase but three phases exist in KPNC: kenaf fiber, PP matrix, and air. Only one KPNC sample was used but an extensive series of tests were conducted to characterize the creep behavior of KPNC.

Creep Behavior

Polymers used in engineering applications are often subjected to stress for a long time and at high temperatures. In this case,

polymers exhibit time-, temperature-, and stress-dependent behavior. Therefore, understanding the viscoelastic properties of polymers is very important. Creep is the progressive deformation of a material at a constant stress. Creep behavior is another very important end-use property for natural fiber–reinforced polymer matrix composites (PMCs), because both the natural fiber reinforcement and polymer matrix exhibit time- and temperature-dependent properties. When performing a creep test, a plastic material deforms continuously. The primary stage is when the creep rate decreases rapidly with time. The initial strain is generally predicted by its elastic stress–strain curve. The material will continue to deform slowly with time. The creep deformation then reaches a steady-state until yielding or rupture. All plastics creep to a certain extent due to their viscoelastic properties. The degree of creep depends on factors such as type of plastic, magnitude of load, temperature, and time.[11–13] There have been considerable studies on the creep behavior of natural fiber-reinforced PMCs[14–18]; however, there is no comprehensive study on the creep behavior of natural fiber nonwoven composites to our best knowledge. In this article, the effects of time, temperature, and stress on the creep behavior of KPNCs and virgin PP plastics were investigated. Two models suitable for evaluating the creep behavior of these materials are discussed. The long-term creep and recovery behavior of these materials are predicted.

Creep and Recovery Models

Many models have been proposed to describe the creep behavior of polymers. The creep behavior is represented by simple rheological models if the polymer is tested under the linear viscoelastic limit (LVL). These models can be divided into physical models and empirical models based on the interpretation of parameters. The four-element Burgers (FEB) model has been widely used as a physical model to capture the creep behavior of natural fiber-reinforced PMCs.[19–21] This model has one Maxwell unit and one Kelvin unit connected in series. The creep strain for PMC consists of three parts: instantaneous deformation resulting from the Maxwell spring; viscoelastic deformation resulting from Kelvin units; and viscous deformation resulting from the Maxwell dashpot. It can be expressed as:[22]

$$\varepsilon(t)=\frac{\sigma}{E_M}+\frac{\sigma}{E_K}[1-\exp(-t/\tau)]+\frac{\sigma}{\eta_M}t,\ \tau=\frac{\eta_K}{E_K} \tag{1}$$

where $\varepsilon(t)$ is the creep strain; σ is the applied stress; t is the time; τ is the retardation time for the Kelvin element to produce 63.21% (or 1–1/e) of its total deformation; E_M and E_K are the elastic moduli of the springs; and η_M and η_K are viscosities of the dashpots in this model. The parameters E_M, E_K, η_M, and η_K can be obtained by fitting experimental data with eq. (1) and can be used for characterization of creep properties. In this equation, the first term is a constant and independent of time; the second term contributes to the early stage of creep, but reaches a maximum quickly; and the last term determines the long-term creep trend at a constant creep rate. Based on the FEB model, the creep rate $\varepsilon'(t)$ can be expressed as:

$$\varepsilon'(t)=\frac{d\varepsilon(t)}{dt}=\frac{\sigma}{\eta_K}\exp\left(\frac{-E_K}{\eta_K}t\right)+\frac{\sigma}{\eta_M} \tag{2}$$

The creep rate reaches to a constant value when the creep reaches a steady state ($t=\infty$), as shown below:

$$\varepsilon'(\infty)=\frac{\sigma}{\eta_M} \tag{3}$$

The Findley power law (FPL) model is one of the most popular empirical models for analyzing creep behavior of polymers. It can be expressed as:[23]

$$\varepsilon(t)=\varepsilon_0+\varepsilon_c\times t^n \tag{4}$$

where $\varepsilon(t)$ is the creep strain at time t; ε_0 is the time-independent initial strain; ε_c is the amplitude of creep strain which is a time-dependent coefficient; n is the time exponent that is independent of stress and is generally less than one; ε_0 and ε_c are functions of stress and environmental variables.

When the constant stress is removed at time t_0, the sample starts to recover, which is the reverse of creep. The maximum deformation is achieved at time t_0:

$$\mathrm{R}(t)=\varepsilon(t_0)-\ \varepsilon(t_0+t) \tag{5}$$

The creep deformation in the recovery process can be divided into two parts: recoverable strain, R(t) at time t, and nonrecoverable strain, NR(t) at time t, as expressed below:

$$\varepsilon(t)=\mathrm{R}(t)+\mathrm{NR}(t) \tag{6}$$

The recoverable strain for the FEB model is:

$$\mathrm{R}(t)=\frac{\sigma}{E_M}+\frac{\sigma}{E_K}\left[1-\exp\left(\frac{E_K}{\eta_K}t\right)\right] \tag{7}$$

The nonrecoverable strain for the FEB model is:

$$\mathrm{NR}(t)=\frac{\sigma}{\eta_M}t \tag{8}$$

The recovery rate at time t is defined as:

$$\mathrm{RR}(t)\%=\frac{\mathrm{R}(t)}{\varepsilon(t)}\times 100\%=100\%-\frac{\mathrm{NR}(t)}{\varepsilon(t)}\times 100\% \tag{9}$$

In the cyclic creep and recovery analysis, the recovery rate of each cycle was calculated using eq. (9). The cyclic creep and recovery experimental data were fitted in an exponential decay model expressed by:

$$\mathrm{RR}(N)=a\times\exp(-N/b)+\mathrm{RR}(\infty) \tag{10}$$

where RR(N) is defined as the recovery rate of the Nth cycle; RR(∞) is defined as the recovery rate after infinite numbers of creep cycles; N is the number of cycles; a is an exponential decay amplitude; and b is a decay constant.

Time-Temperature Superposition

Although long-term creep is very important for evaluating the end-use performance of natural fiber-reinforced composites, it is usually not practical to perform a creep test for an extremely long period of time. Time-temperature superposition (TTS) is one of the most useful extrapolation techniques to predict the long-term creep behavior using short-term testing.[24–26] TTS assumes that the viscoelastic behavior of amorphous polymers at one temperature can be related to that at another temperature by a change in the time scale only. The curves from tests at different temperatures are horizontally shifted along a logarithmic time axis until the curves overlap to form one continuous

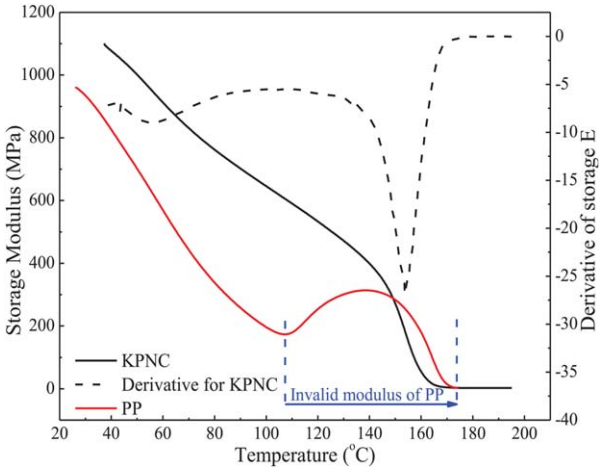

Figure 1. Storage moduli of KPNC and PP as a function of temperature. [Color figure can be viewed in the online issue, which is available at wileyonlinelibrary.com.]

master curve. The TTS technique was originally developed for amorphous polymers. Ward et al.[27] concluded that TTS could not be applied to crystalline polymers because of their complicated thermal behavior. However, Landel et al. [28] suggested that TTS could be applicable to semicrystalline polymers if a vertical shifting factor was also introduced into the TTS method. Since the TTS method has limits to its application,[29] verification of the master curve with a 3-day creep test is necessary to validate this model for KPNCs.

EXPERIMENTAL

Material

The kenaf fiber was supplied by Engage Resources (Thailand), Ltd Co. PP staple fiber, which was supplied by Fiber Science, (Palm Bay, FL) with an average length of 50.8 mm and fineness of 7 denier was used for nonwoven formation and bonding. The PP sample for creep tests was cut from a solid block of virgin PP, which was supplied by Sabic (grade code: 575P, Sittard, The Netherlands). The melt flow rate of the PP sample is 10.5 g /10 min at 230°C and 2.16 kg (ISO 1133). Specimens were 13 ± 1 mm wide and the testing length was fixed at 35 mm. The KPNC specimens were 3.0 ± 0.2 mm thick and solid virgin PP plastics were 1.9 ± 0.1 mm thick.

Nonwoven Composite Fabrication

The manufacture of KPNCs follows the same method in our previous articles.[10,30] This process involves three steps: carding, needle-punching, and thermal compression. The kenaf fiber, which acts as the reinforcement, was manually opened and mixed with PP fibers in 50/50 weight ratio. The mixture was then fed into an F015D Universal Laboratory Carding Machine (Model F015D, SDL Atlas, Rock Hill, SC) to produce a fiber web. During carding, the mixture was further opened and individual fibers were combed to be parallel. The fiber web was carded once again in the perpendicular direction to improve web isotropy. Subsequently, these fibrous felts were transferred to a Laboratory Needle Loom (Model 237, Morisson Benkshire, North Adams, MA) to produce nonwoven felts. The feeding speed is 1.6 m/min and the punching rate is 228 strokes/min. By applying the mechanical needling technology, the fiber blends were greatly entangled and interacted in the out-of-plane direction. After needle-punching, the nonwoven felts are much denser and stronger than the fiber web. Next, the felts were cut into 300 × 300 mm^2 size of segments and machine gauge length was set to 3.175 mm (1/8 inch) for composite thickness control. Samples were compression molded by the MEYER® Transfer Printing and Laboratory Press System-Type APV 3530/16 (Meyer LLC., Roetz, Germany).The KPNC sample that compression molded at 0.5 MPa and 230°C for 60 s was selected for the creep tests. After compression molding, samples were transferred to a pair of cold plates and cold pressed at 0.5 MPa for 30 s to obtain a sleek surface.

Methods

Creep tests were performed using a dynamic mechanical analyzer (DMA) (Model Q800, TA Instrument, New Castle, DE) in the dual-cantilever mode. In each test, the specimens were heated to the desired temperature and were allowed to equilibrate for 5 min prior to the test. Each test was performed three times. The averaged values were reported. The maximum nominal normal stress (MPa) in the dual-cantilever deformation

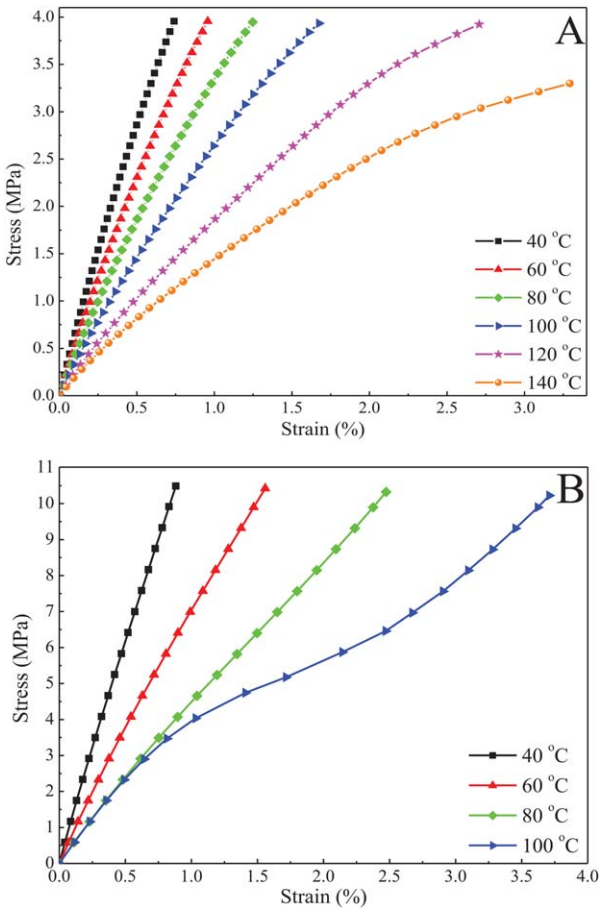

Figure 2. Stress-strain curves for (A) KPNC and (B) PP at various temperatures at a strain rate of 2.28×10^{-5} s^{-1}. The solid lines are interpolations between the data points. [Color figure can be viewed in the online issue, which is available at wileyonlinelibrary.com.]

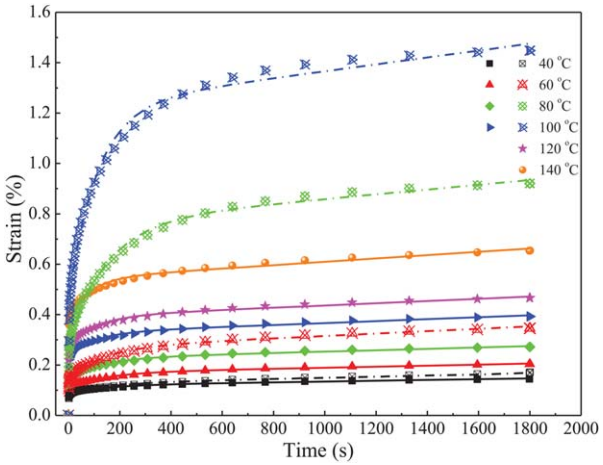

Figure 3. 30-min creep strain for KPNC (solid symbol) and PP (hollow symbol) at various temperatures when $\sigma = 1$ MPa. Symbols represent experimental data and lines represent the FEB model fits. [Color figure can be viewed in the online issue, which is available at wileyonlinelibrary.com.]

mode is calculated using eq. (11) and the maximum nominal normal strain (%) is expressed using eq. (12):

$$\sigma_x = \frac{3 \times P \times L}{w \times t^2} \tag{11}$$

$$\varepsilon_x = \frac{3 \times \delta \times t \times F_c}{L^2 \times \left[1 + \frac{12}{5} \times (1+\upsilon) \times \left(\frac{t}{L}\right)^2\right]} \tag{12}$$

where L is the length (mm) between clamps (17.5 mm in this study); w is the sample width (mm); t is the sample thickness (mm); P is half of the applied force (N); F_c is the clamping correction factor; and υ is the material Poisson's ratio. For KPNC υ is 0.30[10] and for virgin PP υ is 0.45.[31]

Temperature Determination in Creep Tests. To determine the temperature steps to perform creep test, KPNC sample was heated from 40 to 200°C and the virgin PP sample was heated from 40 to 180°C at a heating rate of 5°C/min. The samples were deformed in the dual-cantilever mode at 0.05% strain. Loading frequency was 1.0 Hz.

Linear Viscoelastic Limit. Strain sweep tests of the KPNC and PP samples up to the maximum force level of the instrument (i.e., 18 N) were performed at a frequency of 1 Hz and at the temperatures of 40, 60, 80, 100, 120, and 140°C. The strain rate was 2.28 × 10^{-5} s^{-1}.

Thirty-Minute Creep Tests. The 30-min creep tests were performed at a frequency of 1 Hz at the temperatures of 40, 60, 80, 100, 120, and 140°C for KPNC and at the temperatures of 40, 60, 80, and 100°C for PP. After equilibrating at the desired temperature, a stress of 1 MPa (the LVL value obtained in Linear Viscoelastic Limit section) was applied and held constant for 30 min while the creep strain was measured, followed by a 30-min recovery.

Three-Day Creep Tests. Three-day creep tests were also performed at 40°C for both the KPNC and PP samples at the stress level of 1 MPa. After 72 h, the stress was released and the sample was allowed to recover for 24 h. The three-day creep test results were compared with the TTS prediction from the master curves.

Stress Effects. The 30-min creep tests were performed at a frequency of 1 Hz at 40°C for both KPNC and PP. After equilibrating, five stress levels of 0.5, 1.0, 1.5, 2.5, and 3.5 MPa were applied and held constant for 30 min while the creep strains were measured.

Cyclic Creep Tests. The 30-min creep test in 2.3.3 was repeated for a total of 10 cycles at 40–140°C for KPNC and at 40–100°C for the PP sample. The recovery rate for each cycle was calculated using eq. (9).

Creep Molding and Recovery Analysis. Nonlinear regression was used to estimate E_M, E_K, η_M and η_K values in eq. (1). Least-square estimates of the regression parameters were calculated by minimizing the sum of squares. The correlation coefficient value r^2 is defined as model sum of squares divided by total sum of squares. A better goodness-to-fit is obtained when r^2 is closer to 1. Statistical Analysis System (SAS) version 9.2 (SAS, Cary, NC) was used to perform this nonlinear regression analysis on the experimental data. The Gauss-Newton iterative method was

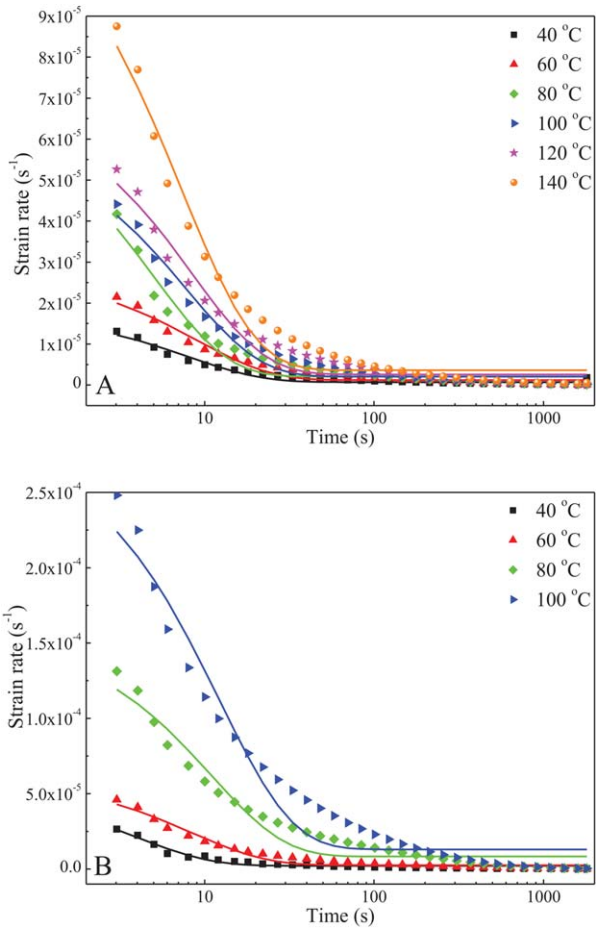

Figure 4. 30-min creep strain rate for (A) KPNC and (B) PP at various temperatures when $\sigma = 1$ MPa. Symbols represent experimental data and lines represent the FEB model fits. [Color figure can be viewed in the online issue, which is available at wileyonlinelibrary.com.]

Table I. The Fitted Parameters Obtained from the Four-Element Burgers Model at $\sigma = 1$ MPa

Sample	T (°C)	E_M (MPa)	E_K (MPa)	η_K (GPa·s)	η_M (GPa·s)	r^2	τ (s)	$\varepsilon'(\infty)$ ($10^{-7}s^{-1}$)
KPNC	40	1161	3058	429	6250	0.995	140.3	1.6
	60	928	1653	224	4762	0.995	135.6	2.1
	80	681	1264	164	3704	0.992	130.0	2.7
	100	422	1096	115	2564	0.991	105.3	3.9
	120	368	834	89	2273	0.992	107.1	4.4
	140	257	652	56	1515	0.990	86.4	6.6
PP	40	978	1996	227	3333	0.992	113.8	3.0
	60	686	818	112	2128	0.993	136.7	4.7
	80	347	210	31	1068	0.995	149.5	9.4
	100	218	130	15	730	0.993	112.1	13.7

implemented in estimating the parameters and minimizing the sum of squares.

RESULTS AND DISCUSSION

Temperature Determination in Creep Tests

As seen in Figure 1, the glass transition of KPNC occurred within 40–60°C and melting of KPNC occurred within 150–160°C. Therefore, the creep test temperature steps of KPNC were selected from 40 to 140°C with an increment of 20°C. In addition, the reference temperature (T_{ref}) in the TTS prediction was selected as 40°C, because it is desirable to set T_{ref} close to T_g. For virgin PP, an abnormal storage modulus bump occurred when temperature exceeded 100°C. Because PP exhibited a very low viscosity above 100°C, the dimensional changes of the PP samples were very significant. Storage modulus calculations assume that the sample behaves in a linearly elastic manner. The creep strain caused by sample gravity was higher than the true strain applied by the instrument. Therefore, valid creep data for the PP sample was obtained by the DMA method only up to 100°C. The creep test temperature steps of PP were, thus, selected from 40 to 100°C, with an increment of 20°C.

Linear Viscoelastic Limit

Figure 2 shows the strain sweep test results for KPNC at 40–140°C and of PP at 40–100°C. The stress-strain curve for KPNC showed a good linear relationship in the testing region up to about 3.5 MPa at 40°C, The LVL of KPNC was shortened to about 1 MPa when the temperature increased to 140°C. This phenomenon resulted from the viscous behavior of KPNC and was not apparent during the test at 40°C. However, the mobility of polymer molecular chains (mainly PP matrix) increased with increasing temperature. Therefore, a stress of 1 MPa was used in the creep tests to ensure that the creep deformations were within the LVL.

Temperature Effects

Figure 3 shows the experimental creep strains as a function of time for KPNC at 40–140°C and for PP at 40–100°C when a constant stress of 1 MPa was applied. The fitted curves from the FEB model are drawn as solid lines for KPNC and dash lines for PP for the purpose of comparison. Overall, the

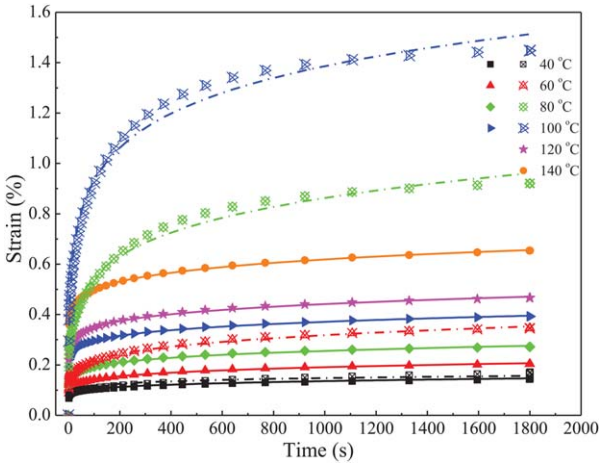

Figure 5. 30-min creep strain for KPNC (solid symbol) and PP (hollow symbol) at various temperatures when $\sigma = 1$ MPa. Symbols represent experimental data and lines represent the FPL model fits. [Color figure can be viewed in the online issue, which is available at wileyonlinelibrary.com.]

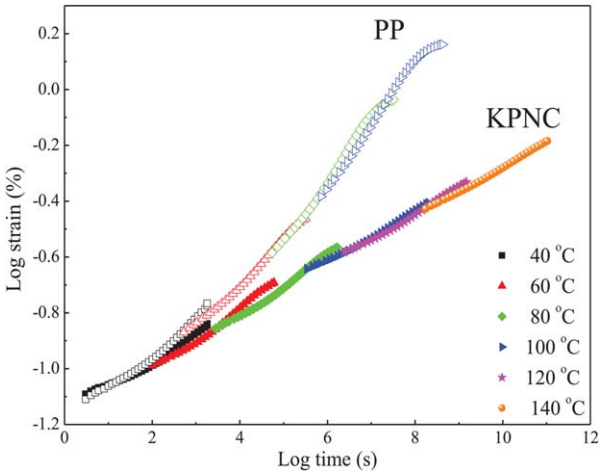

Figure 6. TTS master curves constructed from the 30-min creep data for KPNC (solid symbol) and PP (hollow symbol) at 40, 60, 80, 100, 120 and 140°C ($T_{ref} = 40$°C). [Color figure can be viewed in the online issue, which is available at wileyonlinelibrary.com.]

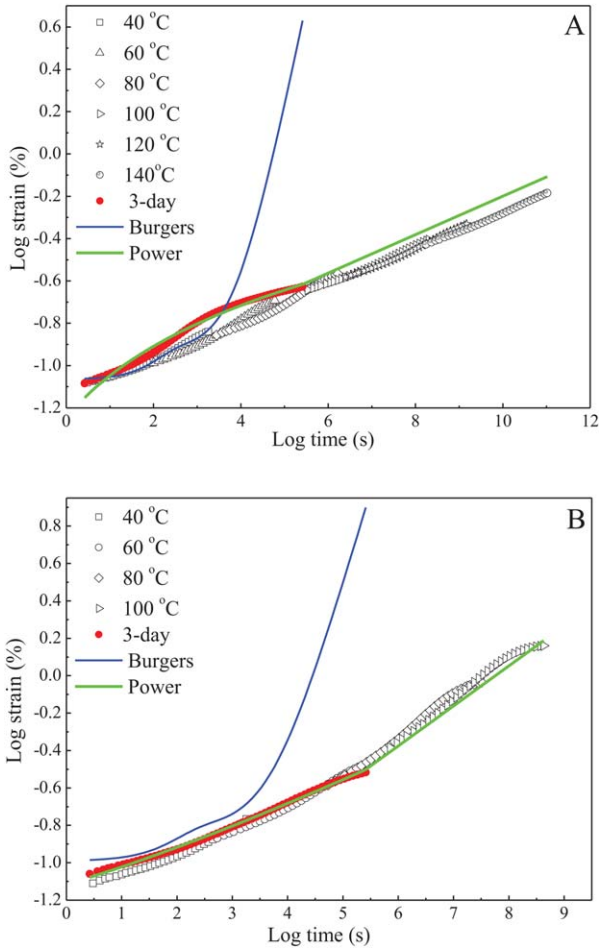

Figure 7. Comparison of three-day creep data with TTS and predictions at 40°C (A) KPNC and (B) PP. Symbols represent experimental data; solid lines represent fits using the FEB model and the FPL model. [Color figure can be viewed in the online issue, which is available at wileyonlinelibrary.com.]

temperature had a statistically significant effect on the creep strains for KPNC and PP (one-way ANOVA, $P < 0.05$). The creep strains for KPNC and PP increased at elevated temperatures. KPNC had a lower creep strain than the virgin PP at each temperature step. The differences on creep strains between KPNC and PP were greater at higher temperatures. Therefore, KPNC showed a better creep resistance than the virgin PP, especially in a high-temperature environment.

Generally speaking, the fitting by FEB model showed good agreement with experimental data at each temperature step, demonstrating that the parameters for the FEB model were applicable to the characterization of KPNC creep properties. However, some discrepancy occurred at the end of the 30-min creep tests. Moreover, the discrepancy became larger at higher temperatures especially for PP at 100°C. The creep rate calculated with the FEB model parameters based on eq. (2) are presented in Figure 4, for a comparison with the experimental creep rate. The FEB model overestimated the long-term creep rate. The FEB model could be improved by incorporating more Kelvin units to make six-, eight-, or high-element Burgers models.

The complete FEB modeling parameters are listed in Table I. As a general trend, all four parameters (E_M, E_K, η_K, and η_M) of KPNC and PP decreased as temperature increased. The decreasing tendency of the E_M and η_M values resulted from a decreased material stiffness with respect to decreased instantaneous modulus and a lower viscosity of the bulk materials at elevated temperatures. The decreasing E_K and η_K values exhibited a higher molecular chain mobility of KPNC and PP at elevated temperatures. KPNC showed a smaller creep rate [$\varepsilon'(\infty)$] than PP, indicating that KPNC had lower long-term creep strain and less temperature dependency than PP.

According to eq. (1), E_M is the instantaneous elastic modulus that is determined by the Maxwell spring. It can be immediately recovered once the stress is removed. E_M also corresponds to the elasticity of the crystallized zones in a semicrystallized polymer. Compared to the amorphous regions, the crystallized zones are subjected to immediate stress due to their higher stiffness. The viscosity of the Maxwell unit η_M represents the nonrecoverable creep deformation and is related to the long-term creep rate. At the molecular level, η_M corresponds to damage in the crystallized zones and irreversible deformation in the amorphous regions. The decrease in η_M implies an increasing deformation of the Maxwell unit at elevated temperatures. The retardant elasticity E_k is associated with the stiffness and the retardant viscosity η_k is coupled with the viscosity of the amorphous regions in the semicrystallized polymer. In this study, it was also found that the elasticity E_k and viscosity η_k of the Kelvin unit decreased with temperature, indicating that the deformation of the Kelvin unit became larger at higher temperatures. As shown in Table I, the η_M values are more than 10 times higher than the η_k values.

Figure 5 shows the experimental creep strains as a function of time for KPNC at 40–140°C and for PP at 40–100°C when a constant stress of 1 MPa was applied. The fits from the FPL model are drawn as solid lines for KPNC and dash lines for PP. The results reveal that the FPL model also fit well the experimental data within the whole range of testing temperature. This suggests that the FPL model would also be feasible in predicting KPNC creep behavior.

For the FEB model, the initial quick and unstable creep deformation in the primary stage is represented by the Maxwell spring and the steady-state creep is represented by the Kelvin unit. The creep rates based on these two units are different. Therefore, the predictions from the FEB model within the transition zone (100–600 s) were faster than the experimental creep rates (Figure 3). In contrast, the FPL does not use four parameters to predict the primary and steady-state creep stages. The predictions from the FPL model within the transition zone were slower than the experimental creep rates (Figure 5). Therefore, the FPL is more effective in predicting the creep behavior of polymers that have no significant transition from primary to steady-state creep stage.

The TTS master curves were constructed from the 30-min creep tests for KPNC and PP. As seen in Figure 6, KPNC and PP had very similar initial creep strains at the beginning of the master curves. The differences on creep strains became larger as time

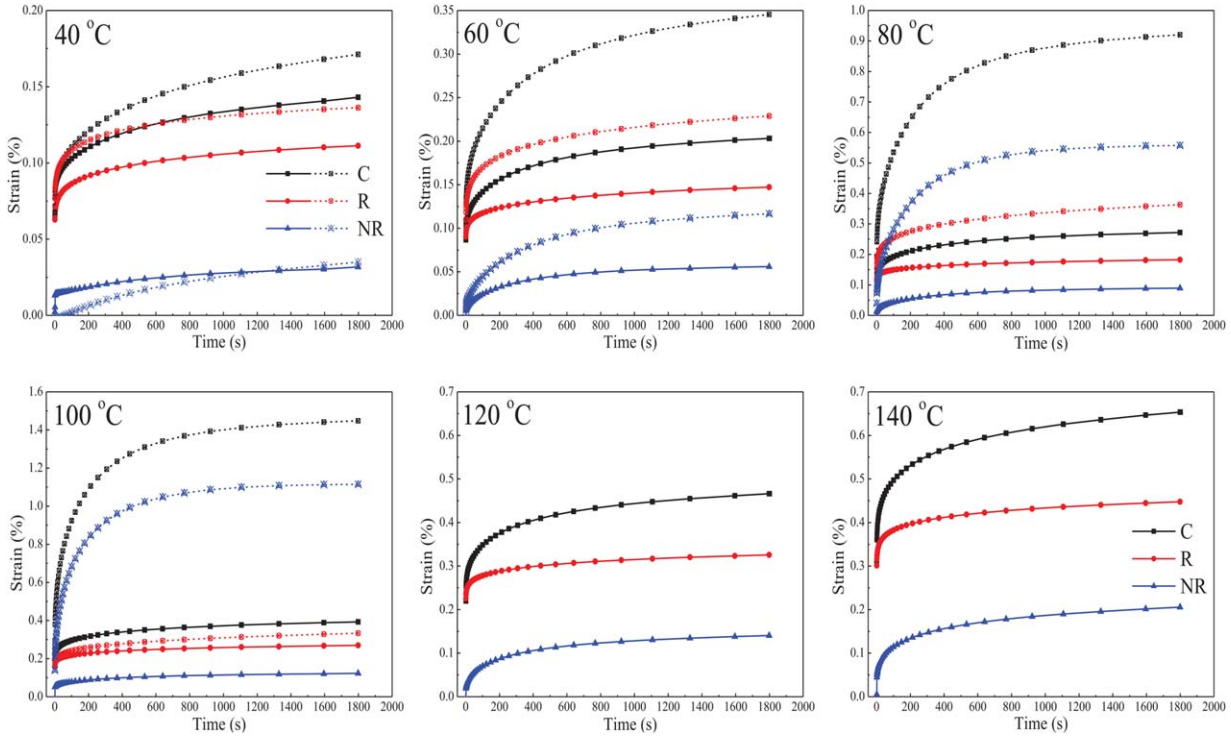

Figure 8. Creep (C), recoverable strain (R), and nonrecoverable (NR) strain for KPNC (solid lines) and PP (dash lines). The lines are interpolations between the data points. [Color figure can be viewed in the online issue, which is available at wileyonlinelibrary.com.]

passed. The one year creep strain was extrapolated from the log creep strain at log time equals to 7.5 in Figure 6. It was estimated to be 0.32% for KPNC and 1.00% for virgin PP at 40°C. KPNC showed both a lower long-term creep strain and a lower creep rate than PP. This resulted from the lower temperature-dependence of KPNC.

Figure 7 shows the comparison between the TTS prediction and the three-day experimental data for KPNC and PP. The TTS prediction for PP fit the three-day experimental data better than KPNC. It can be explained that the solid virgin PP sample had only one phase but KPNC had three phases (kenaf fiber, PP, and air). Therefore, PP was thermorheologically simpler than KPNC. A horizontal shifting was adequate to correctly superimpose the creep data of virgin PP. For KPNC the predicted values from the TTS model were lower than the experimental results. Tajvidi et al.[16] found that the long-term creep strain for 50 wt % kenaf/ HDPE composite was underestimated by the TTS prediction. A better prediction was made by introducing vertical shifts. The difference between the TTS prediction and the experimental data indicated that the master curve needs to be verified before its application, because the creep behavior of polymers, especially semicrystalline polymers, is complicated. They are affected by temperature, stress level, and service conditions.

Although the FEB model fit the 30-min creep test data very well as illustrated in Figure 3, this model can only be used for characterizing short-term creep behavior (30-min creep test in this study). As shown in Figure 7, the prediction of long-term creep behavior for KPNC and PP using the FEB model exhibited a large discrepancy with the three-day experimental data. Xu[32] also pointed out this large discrepancy between the predicted creep strain for 40 wt % bagasse/HDPE composite generated by the FEB model and the three-day creep data. In contrast, the FPL model, as expressed in eq. (4) with ε_0 and ε_c as material constants, showed very good agreement with the three-day experimental data. This indicated that the FPL model was satisfactory for predicting the long-term creep performance of KPNC and PP at 40°C.

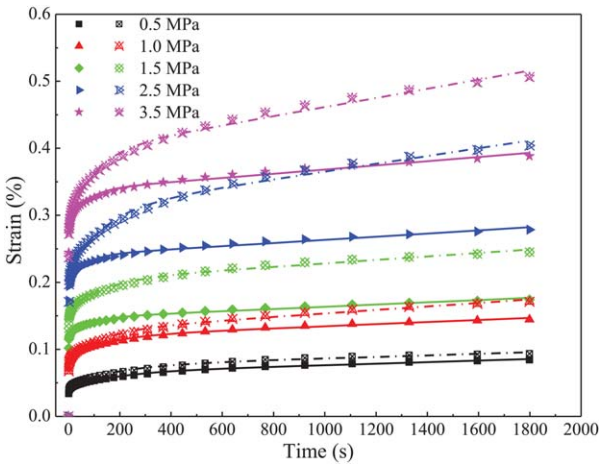

Figure 9. 30-min creep strain for KPNC (solid symbol) and PP (hollow symbol) at various stresses when T= 40°C. Symbols represent experimental data and lines represent the FEB model fits. [Color figure can be viewed in the online issue, which is available at wileyonlinelibrary.com.]

Table II. The Fitted Parameters Obtained from the Four-Element Burgers Model at $T = 40°C$?

Sample	Stress (MPa)	E_M (MPa)	E_K (MPa)	η_K (GPa·s)	η_M (GPa·s)	r^2	τ (s)	$\varepsilon'(\infty)$ ($10^{-7}s^{-1}$)
KPNC	0.5	2415	4292	725	8333	0.995	168.9	1.2
	1.0	1161	3058	429	6250	0.995	140.3	1.6
	1.5	830	3788	301	5882	0.990	79.4	1.7
	2.5	496	2639	175	4167	0.989	66.1	2.4
	3.5	351	1927	125	3226	0.991	64.6	3.1
PP	0.5	2252	3257	593	9091	0.992	182.2	1.1
	1.0	978	1996	227	3333	0.992	113.8	3.0
	1.5	651	2049	261	3846	0.993	127.5	2.6
	2.5	469	1062	143	1724	0.992	134.8	5.8
	3.5	343	978	98	1471	0.991	100.4	6.8

Figure 8 shows the creep, recoverable, and nonrecoverable strains for KPNC and PP based on the 30-min creep tests. The recovery rate denoted as RR (1) at each temperature step is also listed in Table III. The nonrecoverable deformation started from 0 for KPNC at all temperature steps and for PP at 40 and 60°C, indicating that the instantaneous creep deformation was fully recovered for KPNC and for PP at low temperatures. Based on the FEB model, the dashpot in the Maxwell unit created the nonrecoverable strain, which was proportional to creep time as expressed in eq. (8). However, the nonrecoverable curves failed to follow this linear trend, suggesting that the FEB model cannot be applied for recovery prediction. Comparatively, KPNC had lower nonrecoverable deformation than PP at each temperature step. The nonrecoverable deformation was less than the recoverable deformation at each temperature step for KPNC. However, the nonrecoverable deformation was larger than recoverable deformation starting at 80°C for PP. The higher recoverability of KPNC makes it a better choice for a high temperature working environment.

Stress Effects

Figure 9 shows the experimental data for creep strains as a function of time for KPNC and PP when subjected to stress levels of 0.5, 1.0, 1.5, 2.5, and 3.5 MPa at 40°C. The predictions from the FEB model are drawn as solid lines for KPNC and dash lines for PP. Overall, the stress had a statistically significant effect on the creep strains for KPNC and PP (one-way ANOVA, $P < 0.05$). The creep strains for KPNC and PP increased at elevated stress levels. The virgin PP had higher creep strain than KPNC at each stress level. KPNC had better creep resistance than the virgin PP under higher stresses. From Figure 9, it was observed that for both KPNC and PP the creep strain difference was increased corresponding to the stress increases.

The complete FEB modeling parameters are listed in Table II. This model showed good agreement with the experimental data at each stress level. As a general trend, all four parameters (E_M, E_K, η_K, and η_M) of KPNC and PP decreased as temperature increased. One exception is PP at 1.0 and 1.5 MPa. The E_K, η_K, and η_M values at 1.0 and 1.5 MPa did not have statistically significant differences (t test, $P > 0.1$). It is possible that the stress difference of 1.0 and 1.5 MPa is too small to distinguish, considering the fact that the stresses of 1.0 and 1.5 MPa correspond to the forces of 1.9 and 2.8 N applied on the PP sample. At each stress level, KPNC had higher EM values than PP. KPNC also showed a smaller creep rate [$\varepsilon'(\infty)$] than the virgin PP, indicating that the long-term

Table III. The Fitting Parameters for the Cyclic Creep Recovery Rate

Sample	T (°C)	RR (1) (%)	RR (∞) (%)	X	a	b	r^2
KPNC	40	77.78	64.49	0.829	15.58	7.71	0.995
	60	73.44	61.91	0.843	15.78	3.13	0.998
	80	72.38	61.09	0.844	16.44	2.62	0.998
	100	69.78	59.08	0.847	14.02	3.65	0.999
	120	68.50	56.54	0.825	15.89	3.52	0.999
	140	67.13	56.13	0.836	15.06	3.06	0.996
PP	40	78.24	59.87	0.765	24.74	3.13	0.995
	60	51.83	38.26	0.738	21.96	1.97	0.998
	80	39.44	29.22	0.741	16.56	1.96	0.996
	100	23.02	17.30	0.751	10.13	1.69	0.989

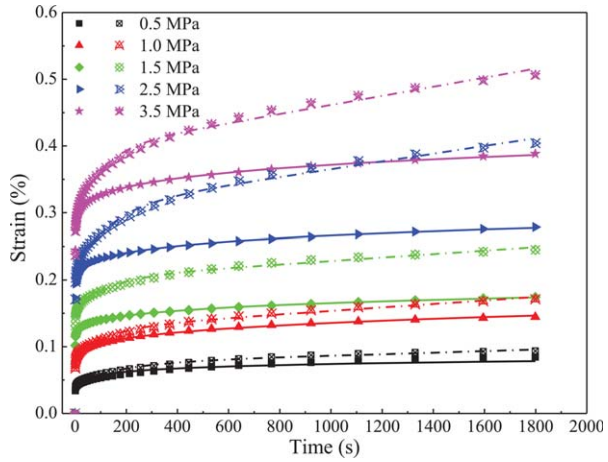

Figure 10. 30-min creep strains for KPNC (solid symbol) and PP (hollow symbol) at various stresses at 40°C. Symbols represent experimental data and lines represent the FPL model fits. [Color figure can be viewed in the online issue, which is available at wileyonlinelibrary.com.]

creep strain of KPNC was lower and less stress-dependent than PP. However, the creep rates of KPNC and PP were insensitive to the stress level of 0.5 MPa at 40°C.

The E_M values of KPNC and PP decreased with increasing stress levels at 40°C. A significant reduction was found at the stresses of 2.5 and 3.5 MPa. Compared to PP, KPNC had a larger E_M value, meaning a higher elasticity, at each temperature step. According to the predictions from the FEB model listed in Table II, both E_K and η_K decreased with an increase in the stress level, indicating that the Kelvin unit had a very high stiffness and was very difficult to flow at low stress levels. With an increase in the stress levels, elastic deformation, and viscous flow became larger, resulting in the reduced E_K and η_K values. The decreases in the E_K and η_K values for KPNC and PP demonstrate the effect of the stress levels on short-term creep resistance. In addition, the reduction of retardation time (τ) at elevated stress levels indicates that the higher stress levels accelerate the transition from primary to secondary creep. Table II also shows that the higher stress level lead to lower η_M values and higher $\varepsilon'(\infty)$ values, reflecting the effect of the stress levels on the long-term creep behavior of KPNC and PP.

To evaluate the FPL model, Figure 10 illustrates the experimental data for creep strains as a function of time for KPNC and PP when subjected to the stress levels of 0.5, 1.0, 1.5, 2.5, and 3.5 MPa at 40°C. The fits from the FPL model are drawn as solid lines for KPNC and dash lines for PP. This model exhibited good agreement with the experimental data at each stress level, demonstrating its applicability in analyzing composite creep behavior.

The time-stress superposition (TSS) master curves were constructed from 30-min creep tests for KPNC and PP (Figure 11). The same method of horizontal shifting as applied to the TTS principle was also used for the TSS master curves by replacing temperature with stress. The effectiveness of the TSS principle has been reported in the literature.[33–36] A phenomenon similar to what was observed from the TTS master curves can be seen in Figure 11. KPNC and PP both exhibited a very similar initial creep strain at the beginning of the master curves. The difference in creep strains became larger as time passed. The extrapolated one-year creep strain is 0.25% for KNPC and 0.40% for

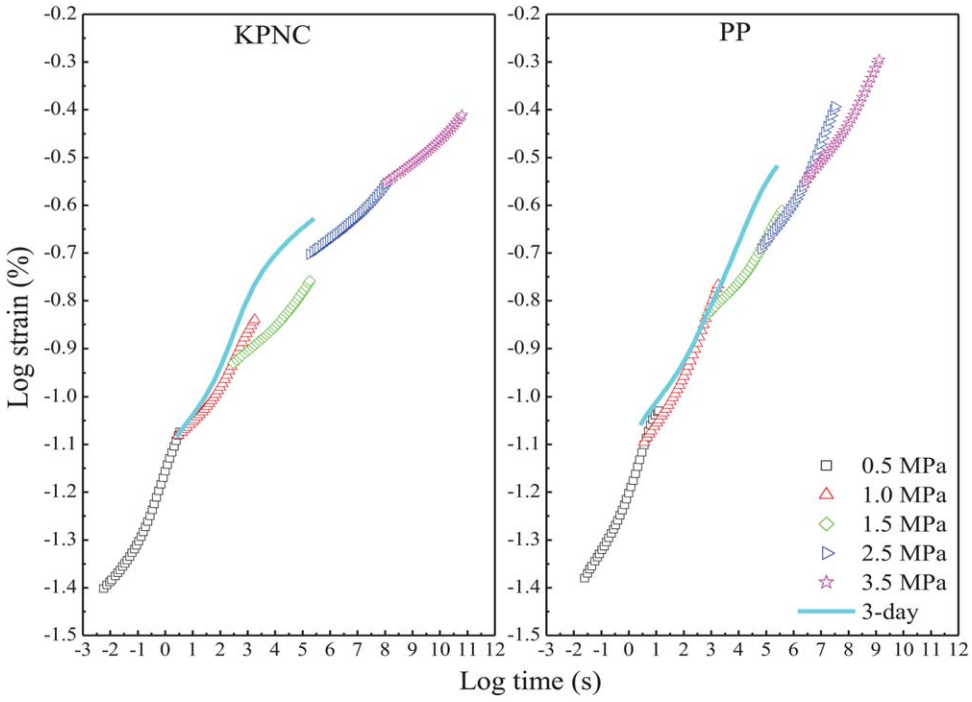

Figure 11. Comparison of TSS master curves constructed from the 30-min creep data at 0.5, 1.0, 1.5, 2.5, and 3.5 MPa ($\sigma_{ref} = 1$ MPa) with three-day creep experimental data (Left) KPNC and (Right) PP. [Color figure can be viewed in the online issue, which is available at wileyonlinelibrary.com.]

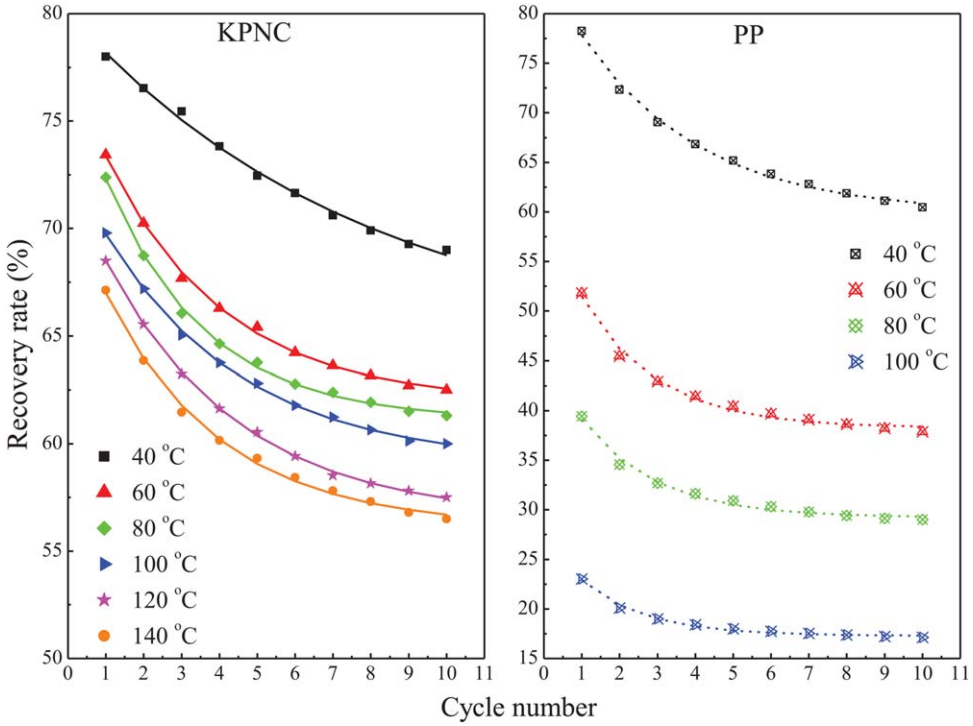

Figure 12. Recovery rate versus cycle number for (Left) KPNC and (Right) PP. Symbols represent calculations from experimental data; lines represent the curve fitting results. [Color figure can be viewed in the online issue, which is available at wileyonlinelibrary.com.]

PP at 1 MPa of the applied stress. KPNC showed a lower long-term creep strain and also a lower creep rate than PP. This resulted from the lower stress-dependence of KPNC. Figure 11 also shows the comparison between the TSS prediction and the three-day creep data of KPNC and PP. The TSS prediction for PP fit the three-day experimental data better than that for KPNC, due to the thermorheologically simplicity of PP as discussed previously. The predicted strains for KPNC from the TSS prediction were lower than the experimental results.

Cyclic Thirty-Minute Creep Tests

Cyclic creep tests were conducted by performing creep tests for 30 min at 1 MPa followed by a 30-min recovery process for 10 cycles. The recovery rate for each cycle was calculated according to eq. (9) and is listed in Figure 12. The exponential decay function expressed in eq. (10) was fit very well with the recovery rates from Cycle 1 to 10. As shown in Table III, the predicted recovery rate of KPNC and PP after infinite numbers of cycles [RR (∞)] decreased at elevated temperatures. At each temperature step, the RR (∞) value of KPNC was higher than PP, indicating a better recoverability of KPNC than PP. X is defined as the ratio of RR (∞) over RR (1). A higher X value indicates a larger percent of recovery rate that materials can retain during the cyclic creep process. KPNC was superior to PP because it maintained a higher recovery rate.

CONCLUSIONS

Both temperature and stress had statistically significant effects on the creep strains for KPNC and PP. The creep strains for KPNC and PP increased at elevated temperatures. However, the creep strain for KPNC was lower than that of PP at each temperature step. The difference on creep strains for KPNC and PP became larger at higher temperatures, indicating that KPNC had a better creep resistance than PP at elevated temperatures. A similar trend was also found on the stress effects. The recovery analyses indicated that KPNC has a higher recovery rate than PP at every 30-min creep cycle.

The FEB model was found only appropriate for characterizing short-term creep behavior (30 min in this study). In contrast, the FPL model was satisfactory for predicting the long-term creep performance of KPNC and PP. Both models demonstrated their applicability in predicting composite creep behavior. However, some limitations of both models still exist.

The TTS master curves for KPNC and PP were established. The master curve for PP fit well with the three-day creep data showing a better prediction accuracy. The master curve for KPNC underestimated its long-term creep performance due to the multiphase thermorheological complexity of KPNC. Therefore, the accuracy of TTS method needs to be verified by experiments (the three-day creep test in this study), especially for composites with multiple components.

ACKNOWLEDGMENTS

The authors would like to thank Prof. Wei Li in the Department of Mechanical Engineering at University of Texas at Austin for the use of the DMA instrument.

REFERENCES

1. Chapman, R. Applications of Nonwovens in Technical Textiles; CRC Press: Boca Raton, FL, **2010**; Chapter 10.

2. Mohanty, A. K.; Misra, M.; Drzal, L. T. *J. Polym. Environ.* **2002**, *10*, 19.
3. Dornburg, V.; Lewandowski, I.; Patel, M. *J. Ind. Ecol.* **2003**, *7*, 93.
4. Pervaiz, M.; Sain, M. M. *Resour. Conserv. Recycl.* **2003**, *39*, 325.
5. Hao, A.; Sun, B.; Qiu, Y.; Gu, B. *Compos. Part Appl. Sci. Manuf.* **2008**, *39*, 1073.
6. Rana, A. K.; Mitra, B. C.; Banerjee, A. N. *J. Appl. Polym. Sci.* **1999**, *71*, 531.
7. Hao, A.; Zhao, H.; Chen, J. Y. *Compos. Part B Eng.* **2013**, *54*, 44.
8. Hao, A.; Zhao, H.; Jiang, W.; Chen, J. Kenaf fiber nonwoven composites as automotive interior material: mechanical, thermal, and acoustical performance. In International SAMPE Technical Conference, Baltimore, MD, May 21–24, **2012**.
9. Holbery, J.; Houston, D. *JOM* **2006**, *58*, 80.
10. Hao, A.; Zhao, H.; Jiang, W.; Yuan, L.; Chen, J. Y. *J. Polym. Environ.* **2012**, *20*, 959.
11. Bledzki, A. K.; Faruk, O. *Compos. Sci. Technol.* **2004**, *64*, 693.
12. Acha, B. A.; Reboredo, M. M.; Marcovich, N. E. *Compos. Part Appl. Sci. Manuf.* **2007**, *38*, 1507.
13. Sullivan, J. L. *Compos. Sci. Technol.* **1990**, *39*, 207.
14. Park, B.-D.; Balatinecz, J. *J. Polym. Compos.* **1998**, *19*, 377.
15. Shi, A.; Wang, L.; Li, D.; Adhikari, B. *Carbohydr. Polym.* **2013**, *96*, 602.
16. Tajvidi, M.; Falk, R. H.; Hermanson, J. C. *J. Appl. Polym. Sci.* **2005**, *97*, 1995.
17. Xu, Y.; Wu, Q.; Lei, Y.; Yao, F. *Bioresour. Technol.* **2010**, *101*, 3280.
18. Pooler, D. J.; Smith, L. V. *J. Thermoplast. Compos. Mater.* **2004**, *17*, 427.
19. Cyras, V. P.; Martucci, J. F.; Iannace, S.; Vazquez, A. *J. Thermoplast. Compos. Mater.* **2002**, *15*, 253.
20. Alvarez, V. A.; Kenny, J. M.; Vázquez, A. *Polym. Compos.* **2004**, *25*, 280.
21. Xu, Y.; Lee, S.-Y.; Wu, Q. *Polym. Compos.* **2011**, *32*, 692.
22. Lee, S.-Y.; Yang, H.-S.; Kim, H.-J.; Jeong, C.-S.; Lim, B.-S.; Lee, J.-N. *Compos. Struct.* **2004**, *65*, 459.
23. Findley, W. N.; Davis, F. Creep and Relaxation of Nonlinear Viscoelastic Materials; Courier Dover Publications: Mineola, NY, **2011**.
24. Pothan, L. A.; Oommen, Z.; Thomas, S. *Compos. Sci. Technol.* **2003**, *63*, 283.
25. Scott, D. W.; Lai, J. S.; Zureick, A.-H. *J. Reinf. Plast. Compos.* **1995**, *14*, 588.
26. Nayak, S. K.; Mohanty, S.; Samal, S. K. *Mater. Sci. Eng. A* **2009**, *523*, 32.
27. Ward, I. M.; Sweeney, J. An Introduction to the Mechanical Properties of Solid Polymers; Wiley: New York, **2005**.
28. Landel, R. F. Mechanical Properties of Polymers and Composites; CRC Press: Boca Raton, FL, **1994**; Vol. *90*.
29. Knauss, W. G. *Mech. Time-Depend. Mater.* **2008**, *12*, 179.
30. Hao, A.; Yuan, L.; Zhao, H.; Jiang, W.; Chen, J. Y. Notch Effects on the Tensile Property of Kenaf/Polypropylene Nonwoven Composites. In ASME 2012 International Mechanical Engineering Congress and Exposition; American Society of Mechanical Engineers: Houston, TX, November 9–15, **2012**, p 593–597.
31. Tscharnuter, D.; Jerabek, M.; Major, Z.; Lang, R. W. *Mech. Time-Depend. Mater.* **2011**, *15*, 15.
32. Xu, Y. Ph.D. Thesis, Louisiana State University: Barton Rouge, LA, **2009**.
33. Urzhumtsev, Y. S. *Polym. Mech.* **1972**, *8*, 438.
34. Starkova, O.; Yang, J.; Zhang, Z. *Compos. Sci. Technol.* **2007**, *67*, 2691.
35. Jazouli, S.; Luo, W.; Bremand, F.; Vu-Khanh, T. *Test* **2005**, *24*, 463.
36. Hadid, M.; Rechak, S.; Tati, A. *Mater. Sci. Eng. A* **2004**, *385*, 54.